CORRECTED 24 DECEMBER 2010; SEE LAST PAGE

virus, for which there may be varying degrees of homotypic and heterotypic immunity (*32*). Secondary infections may occur only when individuals encounter a strain that substantially differs from the one causing primary infection. Furthermore, the true effect of vaccination may differ slightly from that suggested by our model. If vaccination conferred highly protective immunity comparable to that exhibited after two natural infections, our model suggests that the level of herd immunity generated by vaccination could lead to the elimination of the infection from the population at very high coverage levels (*10*). However, one cannot rule out the possible emergence of new rotavirus strains in response to vaccine pressure, and information on rotavirus genetic diversity will be crucial to understand the long-term effectiveness of any immunization program.

We can extend our U.S.-based analysis to the context of developing countries, where rotavirus remains a substantial cause of childhood morbidity and mortality and disease dynamics differ. The high birth rates typical of developing countries may help explain why rotavirus exhibits less seasonal variation in such settings (*33*), although climatic factors could also play a role. In addition, rotavirus vaccine efficacy remains somewhat unclear in developing country settings and could be lower than in the United States because of several factors that might interfere with vaccine performance (e.g., presence of maternal antibodies, high levels of coinfection with other enteropathogens, higher rates of malnutrition, and greater prevalence of uncommon rotavirus strains). Efficacy trials of rotavirus vaccines are ongoing in several countries of Asia and Africa, and results are expected in the next 6 to 12 months. Differences in population demographics, epidemiology of rotavirus disease, and, potentially, vaccine effectiveness, would need to be carefully considered when predicting the benefits of vaccination in developing countries, and the vaccine experience of industrialized nations may not directly translate to countries with high rotavirus mortality burden. Introducing vaccination would likely decrease the overall burden of disease but could have important dynamic consequences, which are key to explore in future research.

References and Notes

1. A. Z. Kapikian, R. M. Chanock, in *Fields Virology*, B. N. Fields *et al.*, Eds. (Lippincott-Raven, Philadelphia, 2001), vol. 2, pp. 1657–1708.
2. U. D. Parashar, C. J. Gibson, J. S. Bresse, R. I. Glass, *Emerg. Infect. Dis.* **12**, 304 (2006).
3. U. D. Parashar, E. G. Hummelman, J. S. Bresee, M. A. Miller, R. I. Glass, *Emerg. Infect. Dis.* **9**, 565 (2003).
4. T. K. Fischer *et al.*, *J. Infect. Dis.* **195**, 1117 (2007).
5. R. I. Glass, U. D. Parashar, *N. Engl. J. Med.* **354**, 75 (2006).
6. R. I. Glass *et al.*, *Lancet* **368**, 323 (2006).
7. G. M. Ruiz-Palacios *et al.*, *N. Engl. J. Med.* **354**, 11 (2006).
8. T. Vesikari *et al.*, *N. Engl. J. Med.* **354**, 23 (2006).
9. A. C. Linhares *et al.*, *Lancet* **371**, 1181 (2008).
10. Materials and methods are available as supporting material on *Science* Online.
11. C. W. LeBaron, J. Lew, R. I. Glass, J. M. Weber, G. M. Ruiz-Palacios, *JAMA* **264**, 983 (1990).
12. T. J. Torok *et al.*, *Pediatr. Infect. Dis. J.* **16**, 941 (1997).
13. R. M. Turcios *et al.*, *Pediatr. Infect. Dis. J.* **25**, 451 (2006).
14. C. Viboud *et al.*, *Science* **312**, 447 (2006); published online 29 March 2006 (10.1126/science.1125237).
15. Y. Xia, O. N. Bjornstad, B. T. Grenfell, *Am. Nat.* **164**, 267 (2004).
16. M. I. Nelson, L. Simonsen, C. Viboud, M. A. Miller, E. C. Holmes, *PLoS Pathog.* **3**, 1220 (2007).
17. M. J. Cox, G. F. Medley, *Epidemiol. Infect.* **131**, 719 (2003).
18. H. Nakajima *et al.*, *Lancet* **357**, 1950 (2001).
19. S. Arista *et al.*, *J. Virol.* **80**, 10724 (2006).
20. S. G. Purohit, S. D. Kelkar, V. Simha, *J. Diarrhoeal Dis. Res.* **16**, 74 (1998).
21. B. T. Grenfell, O. N. Bjornstad, J. Kappey, *Nature* **414**, 716 (2001).
22. A. J. Conlan, B. T. Grenfell, *Proc. R. Soc. London Ser. B* **274**, 1133 (2007).
23. G. Cilla, E. Perez-Trallero, M. C. Lopez-Lopategui, A. Gilsetas, M. Gomariz, *Epidemiol. Infect.* **125**, 677 (2000).
24. B. E. Hamilton, P. D. Sutton, S. J. Ventura, "Revised birth and fertility rates for the 1990s and new rates for Hispanic populations, 2000 and 2001: United States" (National Center for Health Statistics, 2003).
25. Centers for Disease Control and Prevention National Center for Health Statistics, VitalStats, www.cdc.gov/nchs/vitalstats/VitalStatsbirths.htm [accessed 22 April 2008].
26. Agency for Healthcare Quality and Research (AHRQ), www.hcup-us.ahrq.gov/databases.jsp.
27. M. A. Staat *et al.*, *MMWR Morb. Mortal. Wkly. Rep.* **57**, 697 (2008).
28. R. M. Anderson, R. M. May, *Infectious Diseases of Humans: Dynamics and Control* (Oxford Univ. Press, Oxford, 1991).
29. D. I. Bernstein, D. S. Sander, V. E. Smith, G. M. Schiff, R. L. Ward, *J. Infect. Dis.* **164**, 277 (1991).
30. D. L. Smith, B. Lucey, L. A. Waller, J. E. Childs, L. A. Real, *Proc. Natl. Acad. Sci. U.S.A.* **99**, 3668 (2002).
31. D. A. Cummings *et al.*, *Nature* **427**, 344 (2004).
32. B. Jiang, J. R. Gentsch, R. I. Glass, *Clin. Infect. Dis.* **34**, 1351 (2002).
33. S. M. Cook, R. I. Glass, C. W. LeBaron, M. S. Ho, *Bull. World Health Organ.* **68**, 171 (1990).

34. V.E.P and B.G. were supported by NIH (grant R01 GM083983-01) and the Bill and Melinda Gates Foundation. V.E.P, B.G., and L.S. were also supported by the RAPIDD program of the Science and Technology Directorate, U.S. Department of Homeland Security, and the Fogarty International Center, NIH. The findings and conclusions in this report are those of the authors and do not necessarily represent the views of the Centers for Disease Control and Prevention (CDC).

Supporting Online Material

www.sciencemag.org/cgi/content/full/325/5938/290/DC1
Materials and Methods
Figs. S1 to S12
Tables S1 to S4
References

16 February 2009; accepted 3 June 2009
10.1126/science.1172330

Nonlocal Transport in the Quantum Spin Hall State

Andreas Roth,[1] Christoph Brüne,[1] Hartmut Buhmann,[1] Laurens W. Molenkamp,[1]* Joseph Maciejko,[2,3] Xiao-Liang Qi,[2,3] Shou-Cheng Zhang[2,3]

Nonlocal transport through edge channels holds great promise for low-power information processing. However, edge channels have so far only been demonstrated to occur in the quantum Hall regime, at high magnetic fields. We found that mercury telluride quantum wells in the quantum spin Hall regime exhibit nonlocal edge channel transport at zero external magnetic field. The data confirm that the quantum transport through the (helical) edge channels is dissipationless and that the contacts lead to equilibration between the counterpropagating spin states at the edge. The experimental data agree quantitatively with the theory of the quantum spin Hall effect. The edge channel transport paves the way for a new generation of spintronic devices for low-power information processing.

The search for topological states of quantum matter has become an important goal in condensed matter physics. Inside a topological insulator, the conventional laws of electrodynamics are substantially altered (*1*), which may have applications in constructing novel devices for the processing of (quantum) information. The quantum spin Hall (QSH) state (*2*, *3*) is a topologically nontrivial state of matter that exists in the absence of any external magnetic field. It has a bulk energy gap but gapless helical edge states protected by time reversal symmetry. In the QSH regime, opposite spin states forming a Kramers doublet counterpropagate at the edge (*4*, *5*). Recently, the QSH state was theoretically predicted in HgTe quantum wells (*6*). There is a topological quantum phase transition at a critical thickness d_c of the quantum well, separating the trivial insulator state for $d < d_c$ from the QSH insulator state for $d > d_c$. Soon after the theoretical prediction, evidence for the QSH state was observed in transport measurements (*7*). In the QSH regime, experiments measured a conductance G close to twice the quantum unit of conductance $G = 2e^2/h$ (where e is the charge on the electron and h is Planck's constant); this value is consistent with quantum transport due to helical edge states. However, such a conductance quantization in small Hall bar geometries does not allow us to distinguish experimentally between ballistic and edge channel transport in a convincing manner. Thus, it is important to be able to prove experi-

[1]Physikalisches Institut (EP3) and Röntgen Center for Complex Material Systems, Universität Würzburg, Am Hubland, 97074 Würzburg, Germany. [2]Department of Physics, Stanford University, Stanford, CA 94305, USA. [3]Stanford Institute for Materials and Energy Sciences, SLAC National Accelerator Laboratory, 2575 Sand Hill Road, Menlo Park, CA 94025, USA.

*To whom correspondence should be addressed. E-mail: molenkmp@physik.uni-wuerzburg.de

mentally in an unambiguous manner the existence of edge channels in HgTe quantum wells.

Ohm's law versus nonlocal transport. In conventional diffusive electronics, bulk transport satisfies Ohm's law. The resistance is proportional to the length and inversely proportional to the cross-sectional area, implying the existence of a local resistivity or conductivity tensor. However, the existence of edge states necessarily leads to nonlocal transport, which invalidates the concept of local resistivity. Such nonlocal transport has been experimentally observed in the quantum Hall (QH) regime in the presence of a large magnetic field (*8*), and the nonlocal transport is well described by a quantum transport theory based on the Landauer-Büttiker formalism (*9*). These measurements constitute definitive experimental evidence for the existence of edge states in the QH regime.

We report nonlocal transport measurements in HgTe quantum wells that demonstrate the existence of the predicted extended edge channels. We have fabricated structures more complicated than a standard Hall bar that allow a detailed investigation of the transport mechanism. In addition, we present the theory of quantum transport in the QSH regime, and uncover the effects of macroscopic time irreversibility on the helical edge states.

Device structure. We present experimental results on four different devices. The behavior in these structures is exemplary for the ~50 devices we studied. The devices were fabricated from HgTe/(Hg,Cd)Te quantum well structures with well thicknesses of d = 7.5 nm (samples D1, D2, and D3) and 9.0 nm (sample D4). Note that all wells have a thickness $d > d_c \approx 6.3$ nm, and thus exhibit the topologically nontrivial inverted band structure. At zero gate voltage, the samples are n-type and have a carrier density of $n_s \approx 3 \times 10^{11}$ cm^{-2} and a mobility of 1.5×10^5 cm^2 V^{-1} s^{-1}, with small variations between the different wafers. The devices are lithographically patterned using electron-beam lithography and subsequent Ar ion-beam etching. Devices D1 and D2 are micrometer-scale Hall bars with exact dimensions as indicated in the insets of Fig. 1. Devices D3 and D4 are dedicated structures for identifying nonlocal transport, with schematic structure given in Fig. 2. All devices are fitted with a 110-nm-thick Si_3N_4/SiO_2 multilayer gate insulator and a Ti (5 nm)–Au (50 nm) gate electrode stack.

By applying a voltage V_g to the top gate, the electron carrier density of the quantum well can be adjusted, going from an n-type behavior at positive gate voltages through the bulk insulator state into a p-type regime at negative gate voltages. For reasons of comparison, the experimental data in Figs. 1, 3, and 4 are plotted as a function of a normalized gate voltage $V^* = V_g - V_{thr}$ (V_{thr} is defined as the voltage for which the resistance

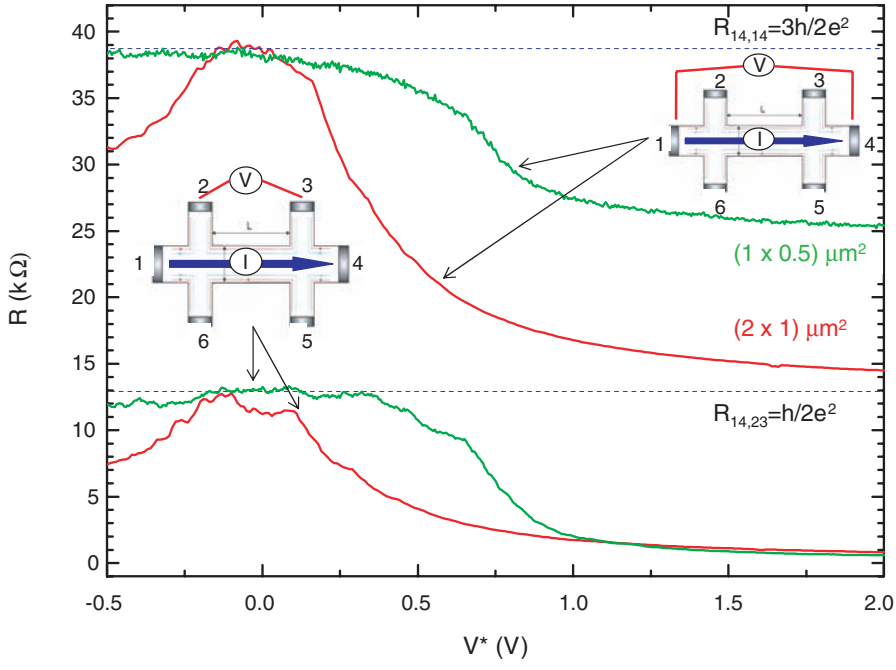

Fig. 1. Two-terminal ($R_{14,14}$) (top two traces) and four-terminal ($R_{14,23}$) (bottom traces) resistance versus (normalized) gate voltage for the Hall bar devices D1 and D2 with dimensions (length × width) as indicated. The dotted blue lines indicate the resistance values expected from the Landauer-Büttiker approach.

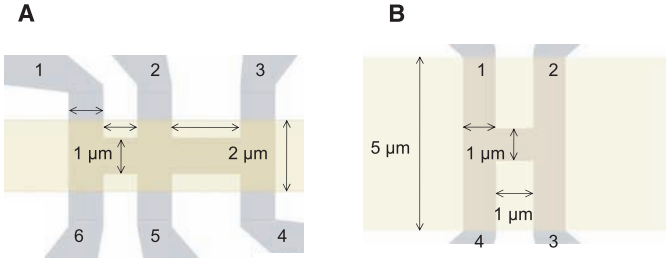

Fig. 2. Schematic layout of devices D3 (**A**) and D4 (**B**). The gray areas are the mesas, the yellow areas the gates, with dimensions as indicated. The numbers indicate the coding of the leads.

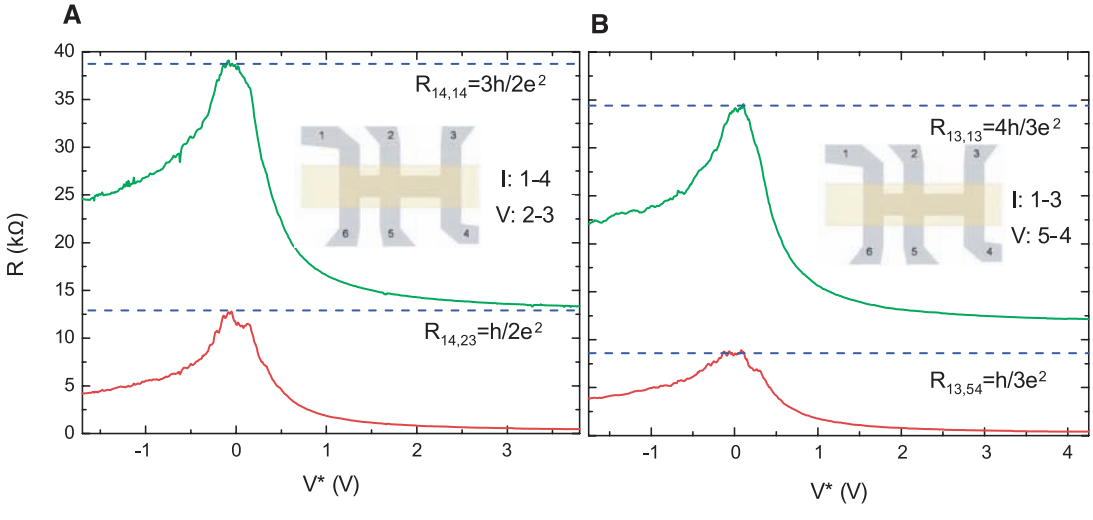

Fig. 3. Four- and two-terminal resistance measured on device D3: (**A**) $R_{14,23}$ (red line) and $R_{14,14}$ (green line) and (**B**) $R_{13,54}$ (red line) and $R_{13,13}$ (green line). The dotted blue lines indicate the expected resistance value from a Landauer-Büttiker calculation.

is largest). Measurements were performed at a lattice temperature of 10 mK for samples D1, D2, and D3 and at 1.8 K for sample D4, using low-frequency (13 Hz) lock-in techniques under voltage bias. The four-terminal resistance (Fig. 1) shows a maximum at about $h/2e^2$, in agreement with the results of (*7*). The contact resistance should be insensitive to the gate voltage and can be measured from the resistance deep in the metallic region. By subtracting the contact resistance, we find that the two-terminal resistance has its maximum at about $3h/2e^2$ (Fig. 1). This value is exactly what is expected from the theory of QSH edge transport obtained from the Landauer-Büttiker formula.

Transport on the edge. Within the general Landauer-Büttiker formalism (*10*), the current-voltage relationship is expressed as

$$I_i = \frac{e^2}{h}\sum_j (T_{ji}V_i - T_{ij}V_j) \qquad (1)$$

where I_i is the current flowing out of the ith electrode into the sample region, V_i is the voltage on the ith electrode, and T_{ji} is the transmission probability from the ith to the jth electrode. The total current is conserved in the sense that $\sum_i I_i = 0$. A voltage lead j is defined by the condition that it draws no net current (i.e., $I_j = 0$). The physical currents are left invariant if the voltages on all electrodes are shifted by a constant amount μ, implying that $\sum_j T_{ij} = \sum_j T_{ji}$. In a time reversal–invariant system, the transmission coefficients satisfy the condition $T_{ij} = T_{ji}$.

For a general two-dimensional sample, the number of transmission channels scales with the width of the sample, so that the transmission matrix T_{ij} is complicated and nonuniversal. However, a tremendous simplification arises if the quantum transport is entirely dominated by the edge states. In the QH regime, chiral edge states are responsible for the transport. For a standard Hall bar with N current and voltage leads attached (compare the insets of Fig. 1 with $N = 6$), the transmission matrix elements for the ν = 1 QH state are given by $T(\mathrm{QH})_{i+1,i} = 1$, for $i = 1, \ldots, N$, and all other matrix elements vanish identically. Here we periodically identify the $i = N + 1$ electrode with $i = 1$. Chiral edge states are protected from backscattering; therefore, the ith electrode transmits perfectly to the neighboring $(i + 1)$th electrode on one side only. In the example of current leads on electrodes 1 and 4, and voltage leads on electrodes 2, 3, 5, and 6, one finds that $I_1 = -I_4 \equiv I_{14}$, $V_2 - V_3 = 0$, and $V_1 - V_4 = (h/e^2)I_{14}$, giving a four-terminal resistance of $R_{14,23} = 0$ and a two-terminal resistance of $R_{14,14} = h/e^2$.

In the case of helical edge states in the QSH regime, opposite spin states form a Kramers pair, counterpropagating on the same edge. The helical edge states are protected from backscattering due to time reversal symmetry, and the transmission from one electrode to the next is perfect. From this point of view, the helical edge states can be viewed as two copies of chiral edge states related by time reversal symmetry. Therefore, the transmission matrix is given by $T(\mathrm{QSH}) = T(\mathrm{QH}) + T^{\dagger}(\mathrm{QH})$, implying that the only nonvanishing matrix elements are given by

$$T(\mathrm{QSH})_{i+1,i} = T(\mathrm{QSH})_{i,i+1} = 1 \qquad (2)$$

Considering again the example of current leads on electrodes 1 and 4 and voltage leads on electrodes 2, 3, 5, and 6, one finds that $I_1 = -I_4 \equiv I_{14}$, $V_2 - V_3 = (h/2e^2)I_{14}$, and $V_1 - V_4 = (3h/e^2)I_{14}$, giving a four-terminal resistance of $R_{14,23} = h/2e^2$ and a two-terminal resistance of $R_{14,14} = 3h/2e^2$. The experimental data in Fig. 1 confirm this picture. For both micro–Hall bar structures D1 and D2 that differ only in the dimensions of the area between voltage contacts 3 and 4, we observe exactly the expected resistance values for $R_{14,23} = h/2e^2$ and $R_{14,14} = 3h/2e^2$ for gate voltages where the samples are in the QSH regime.

Dissipationless transport. Conceptually, one might sense a paradox between the dissipationless nature of the QSH edge states and the finite four-terminal longitudinal resistance $R_{14,23}$, which vanishes for the QH state. We can generally assume that the microscopic Hamiltonian governing the voltage leads is invariant under time reversal symmetry; therefore, one would naturally ask how such leads could cause the dissipation of the helical edge states, which are protected by time reversal symmetry. In nature, the time reversal symmetry can be broken in two ways: at the level of the microscopic Hamiltonian, or at the level of the macroscopic irreversibility in systems whose microscopic Hamiltonian respects the time reversal symmetry. When the helical edge states propagate without dissipation inside the QSH insulator between the electrodes, neither form of time reversal symmetry breaking is present. As a result, the two counterpropagating channels can be maintained at two different quasi–chemical potentials, leading to a net current flow. However, once they enter the voltage leads, they interact with a reservoir containing infinitely many low-energy degrees of freedom, and the time reversal symmetry is effectively broken by the macroscopic irreversibility. As a result, the two counterpropagating channels equilibrate at the same chemical potential, determined by the voltage of the lead. Dissipation occurs with the equilibration process. The transport Eq. 1 breaks the macroscopic time reversal symmetry, even though the microscopic time reversal symmetry is ensured by the relationship $T_{ij} = T_{ji}$. In contrast to the case of QH state, the absence of dissipation of the QSH helical edge states is protected by Kramers' theorem, which relies on the quantum phase coherence of wave functions. Thus, dissipation can occur once the phase coherence is destroyed in the metallic leads. By contrast, the robustness of QH chiral edge states does not require phase coherence. The result of a more rigorous and microscopic analysis on the different role played by a metallic lead in QH and QSH states (*11*) agrees with the simple transport Eqs. 1 and 2. These two equations, which correctly describe the dissipationless quantum transport inside the QSH insulator and the dissipation inside the electrodes, can be subjected to more stringent experimental tests than the two- and four-terminal experiments of Fig. 1 by considering devices D3 and D4 (Fig. 2).

Helical versus chiral. A further difference between helical and chiral edge channels is evident from our experiments on the six-terminal device D3 (Fig. 3). When the longitudinal resistance of device D3 is measured by passing a current through contacts 1 and 4 and by detecting the voltage between contacts 2 and 3 ($R_{14,23}$), we find, similar to the results of Fig. 1, a resistance value of $h/2e^2$ when the bulk of the device is gated into the insulating regime (Fig. 3A). However, the longitudinal resistance is markedly different in a slightly modified configuration, where the current is passed through contacts 1 and 3 and the voltage is measured between contacts 5 and 4 ($R_{13,54}$) (Fig. 3B). We now find $R_{13,54} \approx 8.6$ kilohms, which is markedly different from what one would expect for either the QH transport or the purely diffusive transport, where this configuration would be equivalent to the previous one. Application of Eqs. 1 and 2 actually predicts that the observed behavior is indeed what one expects for helical edge channels. This resistance value can again be expressed as an integer fraction of the inverse conductance quanta e^2/h: $R_{13,54} = h/3e^2$. This result shows that the current through the device is influenced by the number of ohmic contacts in the current path. These ohmic contacts lead to the equilibration of the chemical potentials between the two counterpropagating helical edge channels inside the contact. There are also some devices for which

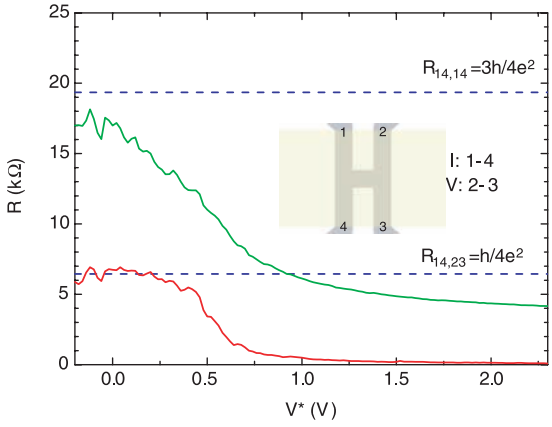

Fig. 4. Nonlocal four-terminal resistance and two-terminal resistance measured on the H-bar device D4: $R_{14,23}$ (red line) and $R_{14,14}$ (green line). Again, the dotted blue line represents the theoretically expected resistance value.

the maximal resistance does not match the theoretical value obtained from Eqs. 1 and 2, but still remains an integer fraction of the quantum h/e^2. This result can be naturally understood as due to inhomogeneities in the gate action (e.g., due to interface trap states) inducing some metallic droplets close to the edge channels while the bulk of the sample is insulating. A metallic droplet can cause dephasing of the electronic wave function, leading to fluctuations in the device resistance. For full dephasing, the droplet plays the role of an additional ohmic contact, just as for the chiral edge channels in the QH regime (*8*). More details on the effects of additional ohmic contacts in the QSH state are given in (*11*).

Another measurement that directly confirms the nonlocal character of the helical edge channel transport in the QSH regime is in Fig. 4, which shows data obtained from device D4, in the shape of the letter H. In this four-terminal device, the current is passed through contacts 1 and 4 and the voltage is measured between contacts 2 and 3. In the metallic n-type regime (low gate voltage), the voltage signal tends to zero. In the insulating regime, however, the nonlocal resistance signal increases to ~6.5 kilohms, which again fits perfectly to the result of Laudauer-Büttiker considerations: $R_{14,23} = h/4e^2 \approx 6.45$ kilohms. Classically, one would expect only a minimal signal in this configuration (from Poisson's equation, assuming diffusive transport, one estimates a signal of about 40 ohms), and certainly not one that increases so strongly when the bulk of the sample is depleted. This signal measured here is fully nonlocal and can be taken (as was done 20 years ago for the QH regime) as definite evidence of the existence of edge channel transport in the QSH regime. A similar nonlocal voltage has been studied in a metallic spin Hall system with the same H-bar geometry (*12*), in which case the nonlocal voltage can be understood as a combination of the spin Hall effect and the inverse spin Hall effect (*13*). The quantized nonlocal resistance $h/4e^2$ we find here is the quantum counterpart of the metallic case. For example, if we assume that the chemical potential in contact 1 is higher than that in contact 4 (compare to the layout of D4 in Fig. 2B), more electrons will be injected into the upper edge state in the horizontal segment of the H-bar than into the lower edge state. Because on opposite edges the right-propagating edge states have opposite spin, this implies that a spin-polarized current is generated by an applied bias $V_1 - V_4$, comparable to a spin Hall effect. When this spin-polarized current is injected into the right leg of the device, the inverse effect occurs. Electrons in the upper edge flow to contact 2 while those in the lower edge flow to contact 3, establishing a voltage difference between those two contacts due to the charge imbalance between the edges. The right leg of the device thus acts as a detector for the injected spin-polarized current, which corresponds to the inverse spin Hall effect.

Concluding remarks. The multiterminal and nonlocal transport experiments on HgTe microstructures in the QSH regime demonstrate that charge transport occurs through extended helical edge channels. We have extended the Landauer-Büttiker model for multiterminal transport in the QH regime to the case of helical QSH edge channels and have shown that this model convincingly explains the observations. Logic devices based on the complementary metal oxide semiconductor design generate considerable heating due to the ohmic dissipation within the channel. Our work on conductance quantization demonstrates that electrons can be transported coherently within the edge channel without ohmic dissipation. Such an effect can be used to construct logic devices with improved performance.

References and Notes

1. S. C. Zhang, *Physics* **1**, 6 (2008).
2. C. L. Kane, E. J. Mele, *Phys. Rev. Lett.* **95**, 226801 (2005).
3. B. A. Bernevig, S. C. Zhang, *Phys. Rev. Lett.* **96**, 106802 (2006).
4. C. Wu, B. A. Bernevig, S. C. Zhang, *Phys. Rev. Lett.* **96**, 106401 (2006).
5. C. Xu, J. Moore, *Phys. Rev. B* **73**, 045322 (2006).
6. B. A. Bernevig, T. L. Hughes, S.-C. Zhang, *Science* **314**, 1757 (2006).
7. M. König *et al*., *Science* **318**, 766 (2007); published online 19 September 2007 (10.1126/science.1148047).
8. C. W. J. Beenakker, H. van Houten, *Solid State Phys.* **44**, 1 (1991).
9. M. Büttiker, *Phys. Rev. B* **38**, 9375 (1988).
10. M. Büttiker, *Phys. Rev. Lett.* **57**, 1761 (1986).
11. See supporting material on *Science* Online.
12. C. Brüne *et al*., http://arxiv.org/abs/0812.3768 (2008).
13. E. M. Hankiewicz, L. W. Molenkamp, T. Jungwirth, J. Sinova, *Phys. Rev. B* **70**, 241301(R) (2004).

14. We thank T. Beringer, N. Eikenberg, M. König, and S. Wiedmann for assistance in some of the experiments. Supported by Deutsche Forschungsgemeinschaft grant SFB 410; German-Israeli Foundation grant I-881-138.7/2005; NSF grant DMR-0342832; the Alexander von Humboldt Foundation; the U.S. Department of Energy, Office of Basic Energy Sciences, under contract DE-AC03-76SF00515; the Focus Center Research Program (FCRP) Center on Functional Engineered Nanoarchitectonics; the National Science and Engineering Research Council of Canada; and the Stanford Graduate Fellowship Program. Computational work was made possible by the facilities of the Shared Hierarchical Academic Research Computing Network (www.sharcnet.ca).

Supporting Online Material

www.sciencemag.org/cgi/content/full/325/5938/294/DC1
SOM Text
Figs. S1 to S9
Table S1
References

8 April 2009; accepted 11 June 2009
10.1126/science.1174736

REPORTS

Higher-Order Photon Bunching in a Semiconductor Microcavity

M. Aßmann,[1] F. Veit,[1] M. Bayer,[1]* M. van der Poel,[2] J. M. Hvam[2]

Quantum mechanically indistinguishable particles such as photons may show collective behavior. Therefore, an appropriate description of a light field must consider the properties of an assembly of photons instead of independent particles. We have studied multiphoton correlations up to fourth order in the single-mode emission of a semiconductor microcavity in the weak and strong coupling regimes. The counting statistics of single photons were recorded with picosecond time resolution, allowing quantitative measurement of the few-photon bunching inside light pulses. Our results show bunching behavior in the strong coupling case, which vanishes in the weak coupling regime as the cavity starts lasing. In particular, we verify the *n* factorial prediction for the zero-delay correlation function of *n* thermal light photons.

The discovery of two-photon bunching in thermal light by Hanbury Brown and Twiss (*1*) marked a turning point for the development of quantum optics (*2*) and has also found applications in a variety of fields, from particle physics (*3*) to ultracold quantum gases (*4*). Photon bunching is the tendency of indistinguishable photons, emitted by a thermal or chaotic light source, to show an enhanced joint detection probability compared with statistically independent particles that are emitted, for instance, by lasers. The explanation of this bunching relies on quantum interference between indistinguishable *n* particle probability amplitudes leading to excess joint detections if the photon number follows the Bose-Einstein distribution (*5*, *6*).

The quantity describing bunching for two photons is the second-order intensity correlation function defined as

$$g^{(2)}(t,\tau) = \frac{\langle :\hat{n}(t)\hat{n}(t+\tau): \rangle}{\langle \hat{n}(t) \rangle \langle \hat{n}(t+\tau) \rangle} \qquad (1)$$

where $\hat{n} = \hat{a}^{\dagger}\hat{a}$ is the photon number operator, t and $t + \tau$ are the detection times of the two

[1]Experimentelle Physik II, Technische Universität Dortmund, D-44221 Dortmund, Germany. [2]DTU Fotonik, Technical University of Denmark, DK-2800 Kongens Lyngby, Denmark.

*To whom correspondence should be addressed: E-mail: manfred.bayer@tu-dortmund.de

ERRATUM

Post date 24 December 2010

Research Articles: "Nonlocal transport in the quantum spin Hall state" by A. Roth *et al.* (17 July 2009, p. 294). An unintended duplication of figure elements was introduced during manuscript preparation. Despite their different horizontal scales, the red $R_{14,23}$ curve in Fig. 1 is the same as that in Fig. 3A; likewise, the red $R_{14,14}$ curve in Fig. 1 is the same as the green curve in Fig. 3A. The configuration of current contacts and voltage probes shown in Fig. 3A is fully equivalent to the four- and two-terminal configurations of a standard Hall bar as shown in Fig. 1. Therefore, this unintended duplication does not affect any claims in the paper. A corrected version of Fig. 1, based on data taken from a Hall bar device different from the one shown in Fig. 3A, is shown here. The original caption is correct.

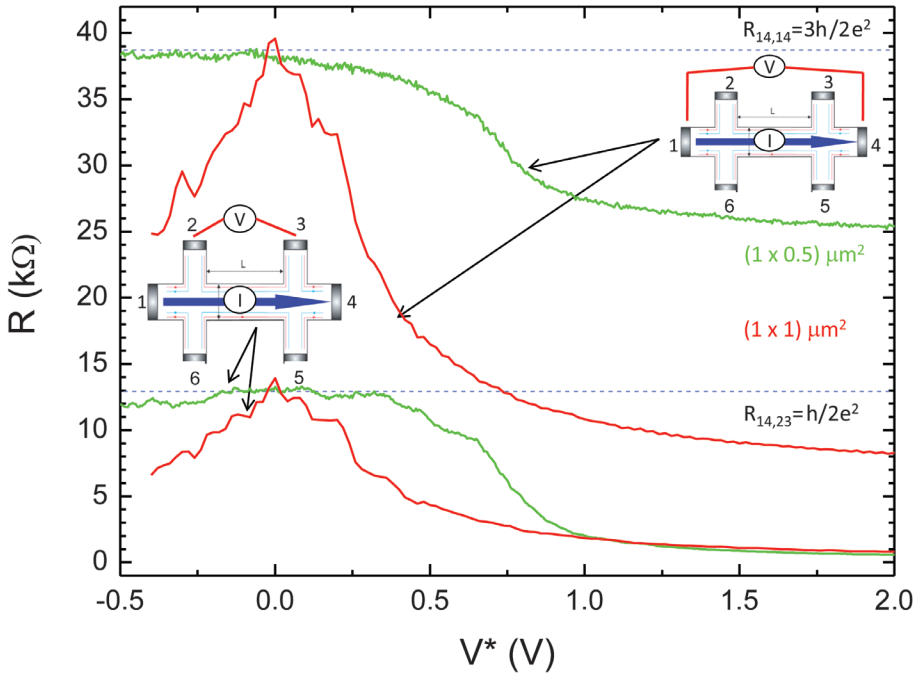

Nonlocal Transport in the Quantum Spin Hall State

Andreas Roth, Christoph Brüne, Hartmut Buhmann, Laurens W. Molenkamp, Joseph Maciejko, Xiao-Liang Qi, and Shou-Cheng Zhang

Science, 325 (5938), • DOI: 10.1126/science.1174736

Living on the Edge

Topological insulators are a recently described state of matter in which the bulk material is an insulator but with a metallic surface state that is protected by the topology of the Fermi surface. Roth *et al.* (p. 294; see the Perspective by Büttiker) now show that the current flow on the surface takes place in edge states around the boundary of the sample. These are similar to the current transport in high-quality two-dimensional electron gases in high magnetic field, which confirms theoretical work on these materials.

Science (ISSN 1095-9203) is published by the American Association for the Advancement of Science. 1200 New York Avenue NW, Washington, DC 20005. The title *Science* is a registered trademark of AAAS.

Given that user fatigue limits the number of interactions, one must make the most of what little data the user provides. The main approach to this is to automate most design evaluations and only selectively query the user. For parameterized design spaces (*11*), function approximation techniques can be used to assign a goodness score, based on similar designs evaluated by the user. But creating an adequate approximation is difficult, and this approach does not generalize to more open-ended, generative representations (*11*) for encoding designs. Another approach—using mathematical heuristics of aesthetics—has found some success in the interactive evolution of jewelry (*12*). The most promising long-term approach is to continuously learn and refine a model of user preferences (*13*) while simultaneously using this model to perform most evaluations.

The interactive systems described above explicitly present the user with choices to select from. Interactive evolutionary algorithms on the Web can also be invisible to the user. For example, the company SnapAds (www.snapads.com) uses an implicit interactive evolutionary algorithm to evolve banner ads. Variations of an ad are placed on Web pages. On the basis of click-through rates, the ad layout evolves and is optimized over the course of a few days. With this approach, the company has improved click-through rates by as much as 1900% (*14*). The challenge in extending such implicit algorithms to other Web applications will be to convert user interactions into a fitness assignment.

As interactive evolutionary algorithms improve and are adopted by Web site developers, we expect them to become increasingly useful for adding intelligence to interactive Web sites. Web sites with explicit interactive evolutionary algorithms could allow users to custom-design products by interactively browsing through virtual catalogs that evolve as users surf through them. Implicit algorithms could enable search engines to adaptively improve their responses to search queries over time and produce user-customized responses. This intelligent Web of the future will not just be powered by better algorithms, but will emerge from the interactions of millions of online users.

References and Notes

1. K. A. De Jong, *Evolutionary Computation: A Unified Approach* (MIT Press, Cambridge, MA, 2006).
2. T. Wajima, M. Matsumoto, S. Sekino, *Hitachi Rev.* **54**, 161 (2005).
3. J. D. Lohn, G. S. Hornby, D. S. Linden, *Artif. Intell. Eng. Des. Anal. Manuf.* **22**, 235 (2008).
4. R. Dawkins, *The Blind Watchmaker* (Norton, New York, 1986).
5. K. Sims, *SIGGRAPH 91 Conference Proceedings, Annual Conference Series* (ACM Press, New York, 1991), pp. 319–328.
6. S. Todd, W. Latham, *Evolutionary Art and Computers* (Academic Press, Orlando, FL, 1992).
7. J. Frazer, *An Evolutionary Architecture* (Architectural Association Publications, London, 1995).
8. J. A. Biles, *Proceedings of the International Computer Music Conference* (ACMA, San Francisco, 1994), pp. 131–137.
9. M. Witbrock, S. Neil-Reilly in *Evolutionary Design by Computers*, P. J. Bentley, Ed. (Morgan Kaufmann, San Francisco, 1999), chap. 10.
10. H. Takagi, *Proc. IEEE* **89**, 1275 (2001).
11. A parameterized representation is like a blueprint in which the parameter values specify dimensions; for example, a table has the parameters of height, width, and depth of the top, plus additional parameters for the dimensions of the legs. A generative representation is a more expressive type of representation and—in contrast to the parameterized representation—allows for the topology of a design to be changed.
12. S. Wannarumon, E. L. J. Bohez, K. Annanon, *Artif. Intell. Eng. Des. Anal. Manuf.* **22**, 19 (2008).
13. T. Kurtoglu, M. I. Campbell, *Res. Eng. Des.* **20**, 59 (2009).
14. See www.snapads.com/casestudies.php.

15. Supported in part by NSF Creative-IT grant 0757532.

10.1126/science.1174400

PHYSICS

Edge-State Physics Without Magnetic Fields

A novel class of materials called topological insulators allows spin physics to be probed without the need for magnetic fields.

Markus Büttiker

Solids can be divided into conductors and insulators. A new class of materials, called topological insulators, has been predicted (*1*, *2*) that exhibit surface states that lead to quantized conductance of charge and spin. These surface states are helical edge states, which interconnect spin and momentum of the carriers. Observation of these states should not require application of a magnetic field. On page 294 of this issue, Roth *et al*. (*3*) present compelling experimental evidence for such helical edge states at the surface of a topological insulator—in this case, quantum wells of mercury telluride (HgTe). Related effects are seen in the quantum Hall effect, but only in the presence of high magnetic fields. In the quantum Hall effect, a magnetic field induces cyclotron motion of electrons that is essential for the formation of edge states.

In the band picture of solids, conduction in materials depends on where the chemical potential μ falls. In metals, it lies in the conduction band, but in insulators, it is at a lower energy and falls into the band gap between the valence and conduction bands. Topological insulators (*1*, *2*) are band insulators with particular symmetry properties arising from spin-orbit interactions. According to theory, the surface edge states should reflect the nontrivial topological properties of the band structure, leading to unidirectional carrier motion along the sample boundary. For the system to be time-invariant, the states must come in pairs so that along a horizontal bar of the material, each edge has a set of states allowing propagation to the left, and another allowing propagation to the right (see the figure, panel A).

At equilibrium, when both states of the pairs are equally populated, there is no net charge current. However, carriers moving to the right could all have spins pointing up and carriers moving to the left might all have spins pointing down. This situation would lead to a net circulating spin current that persists at equilibrium. Such a robust effect normally requires an applied magnetic field.

When a potential is applied, a net carrier flow is set up through a non-equilibrium population of edge states. In panel A of the figure, the flow is to the right, and the greater population of states is depicted with a thicker line.

The closest analog to this system is the quantum Hall effect in a two-dimensional electron gas, in which the bulk is insulating but the sample edge has chiral states that describe electron motion along the sample boundaries. The situation is particularly simple in the integer quantum Hall effect, where each edge has an integer number of states, all of which carry charge in the same direction independent of the spin directions

Department of Theoretical Physics, University of Geneva, 24 Quai E. Ansermet, 1211 Geneva, Switzerland. E-mail: markus.buttiker@unige.ch

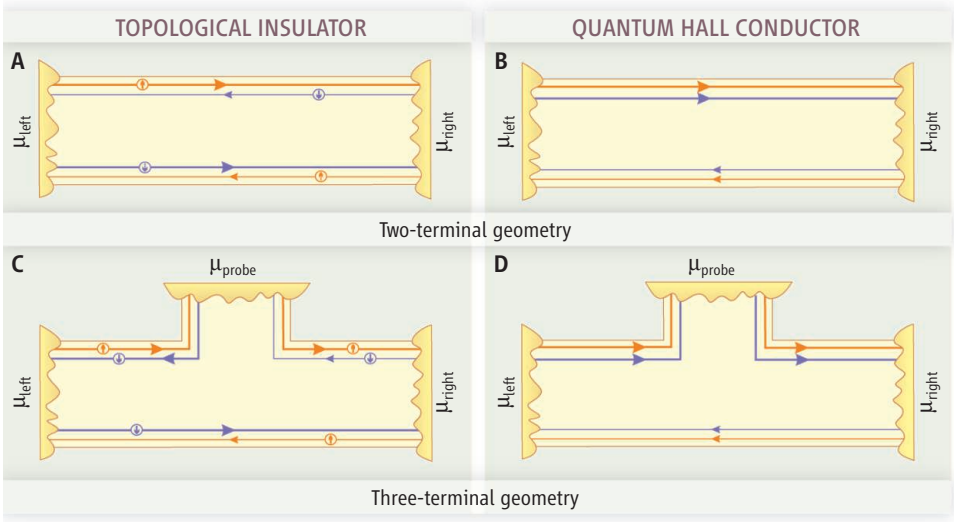

Different at the edges. Both topological insulators (**A** and **C**) and quantum Hall conductors (**B** and **D**) have edge states that connect adjacent contacts. For the topological insulator in (A), the edge states are in pairs that allow spin transport (red, spin up; blue, spin down). In all these examples, the higher chemical potential for the left contact (μ_{left}) leads to transport to the right. In the presence of transport, thick lines show greater occupancy of the states, versus the thin lines showing the unoccupied channels. The topological insulator has states with high occupancy on both sides of the sample, whereas in the quantum Hall conductor, states with higher occupation occur only on one side (B). Adding a probe with chemical potential (μ_{probe}) has no effect for the quantum Hall conductor in (D), but for the topological insulator, a current flows back from the probe to the left contact, cutting the overall conductance by half a conductance quantum (C).

but determined by the applied magnetic field (see the figure, panel B). This system has the same conductance as the topological insulator, but the two edge states that transport current in the integer quantum Hall effect are on the same (upper) side of the sample. In contrast, in the topological insulator, there is one edge state on each side of the sample (see the figure, panel A).

Molenkamp and co-workers provided experimental evidence for topological insulators (*4*) by measuring a conductance consistent with the theoretically predicted number of edge states. However, it remained to be shown that the observed conductance measurements arose from edge states. Roth *et al*. now show changes in conductance caused by a voltage probe. The theoretical predictions are based on a simple application of the scattering theory of multiprobe conductance (*5*) to topological insulators with multiple contacts.

The main effect can be understood by considering the conductance of a three-probe conductor, with one contact playing the role of a voltage probe (*1*). At such a contact, the net current vanishes. Electrons that leave the conductor are replaced by electrons from the contact reservoir. In the quantum Hall effect sample, two edge states from the left source contact enter the voltage probe, and two edge states leave the probe to the right drain contact (see the figure, panel D). The potential of the probe is equal to that of the source contact, and the voltage probe has no effect on the overall conductance.

The situation is very different for a topological insulator (see the figure, panel C). Here, only one edge state is directed from the source contact to the voltage probe. Two other edge states lead away from the probe—one to the source contact and one to the sink contact. To maintain zero current, it is sufficient to tune the chemical potential at the probe halfway between the potentials of the source and sink contact. Now, half the current is directed back to the source contact (a channel that was not populated in the two-terminal geometry in panel A). The voltage probe reduces the overall conductance by half a conductance quantum. Roth *et al*. observed this effect in several different multiprobe geometries.

In the topological insulator, a voltage probe that maintains zero charge current provides momentum relaxation, because it forces half the carriers back against their direction of incidence. Such a probe maintains zero net charge current into the contact. However, the spin current into the probe is nonzero and net spin up in the case depicted. Simultaneously, a spin current is induced into both the source and drain electrodes.

Conceptually, we could ask for a probe that nullifies both the charge and the spin current. It would require separate potentials for spin-up and spin-down carriers. It would, in analogy to the quantum Hall effect, have no effect on conductance. The spin-up potential would be equal to the source contact and the spin-down potential equal to the sink contact. Only one edge state would be filled along both the upper and lower edges. Experiments that relied on unequally populated edge states (*5*) were used almost 20 years ago to prove the physical reality of edge states in the quantum Hall effect (*6*–*8*).

Much of the physics of topological insulators is still under active investigation. Weak disorder has no effect, but strong disorder has been found theoretically to lead to a new phase (*9*) termed a "topological Anderson insulating state." The material used by Roth *et al*. is not the only topological insulator being explored. Martin *et al*. have proposed (*10*) that applying gates to bilayer graphene should generate edge states that are wide relative to the underlying lattice constants of graphene. Topological states may also exist at the interface of ferromagnets and superconductors deposited on top of a topological insulator (*11*, *12*). Such heterostructures could be used to generate qubits (the working states of quantum computers) that are largely immune to the limiting effects of decoherence.

Edge states can be used to direct electrons from one place to another, in a manner similar to directing beams of photons with optics. Such capabilities are of interest in quantum information and quantum processing. The first steps in this direction will be the realization in topological insulators of basic building blocks such as quantum point contacts, Mach-Zehnder interferometers, and the demonstration of two-particle effects (*13*, *14*) without the use of a magnetic field.

References

1. C. L. Kane, E. J. Mele, *Phys. Rev. Lett.* **95**, 226801 (2005).
2. B. A. Bernevig, T. L. Hughes, S.-C. Zhang, *Science* **314**, 1757 (2006).
3. A. Roth *et al.*, *Science* **325**, 294 (2009).
4. M. König *et al.*, *Science* **318**, 766 (2007); published online 19 September 2007 (10.1126/science.1148047).
5. M. Büttiker, *Phys. Rev. B* **38**, 9375 (1988).
6. S. Komiyama *et al.*, *Phys. Rev.* B **40**, 12566 (1989).
7. B. J. van Wees *et al.*, *Phys. Rev. Lett.* **62**, 1181 (1989).
8. B. W. Alphenaar *et al.*, *Phys. Rev. Lett.* **64**, 677 (1990).
9. J. Li, R.-L. Chu, J. K. Jain, S.-Q. Shen, *Phys. Rev. Lett.* **102**, 136806 (2009).
10. I. Martin, Ya. M. Blanter, A. F. Morpurgo, *Phys. Rev. Lett.* **100**, 036804 (2008).
11. L. Fu, C. L. Kane, *Phys. Rev. Lett.* **102**, 216403 (2009).
12. A. R. Akhmerov, J. Nilsson, C. W. J. Beenakker, *Phys. Rev. Lett.* **102**, 216404 (2009).
13. P. Samuelsson, E. V. Sukhorukov, M. Büttiker, *Phys. Rev. Lett.* **92**, 026805 (2004).
14. I. Neder *et al.*, *Nature* **448**, 333 (2007).

10.1126/science.1177157

Edge-State Physics Without Magnetic Fields

Markus Büttiker

Science, 325 (5938), • DOI: 10.1126/science.1177157